ИНСТИТУТ ЯДЕРНОЙ ФИЗИКИ
СО АН СССР

L.M.Barkov, V.I.Kotov,
P.K.Lebedev, L.A.Makarina,
A.P.Mishakova, V.S.Okhapkin,
R.A.Rzaev, V.P.Sakharov,
S.S.Shimansky, V.P.Smakhtin,
M.S.Zolotorev

HADRON-PRODUCTION BELOW 2 GeV/c IN PROTON-NUCLEUS COLLISION AT 70 GeV

PREPRINT 82-42

Новосибирск

HADRON-PRODUCTION BELOW 2 GeV/s IN PROTON-NUCLEUS COLLISION AT 70 GeV

L.M.Barkov, V.I.Kotov*, P.K.Lebedev,
L.A.Makarina+, A.P.Mishakova+, V.S.Okhapkin,
R.A.Rzaev*, V.P.Sakharov*, S.S.Shimansky,
V.P.Smakhtin, M.S.Zolotorev

Institute of Nuclear Physics
630090, Novosibirsk 90, USSR

A b s t r a c t

The production cross sections of pions, protons and anti-protons at zero angle were measured in collision of 70 GeV protons with Al and W targets. The measurements were performed at secondary momentum values equal to 0.4,0.6,0.8,1.07 and 2.0 GeV/c. Pellicles of nuclear emulsion were used to detected and to identity the particles in the secondary beam.

* - Institute of High Energy Physics, Serpukhov

+ - Kurchatov Institute of Atomic Energy, Moscow

1. Introduction

Last years high energy hadron interaction with atomic nuclei attracts a considerable attention /see, for example, reviews 1÷3 and references therein/. This is due to the possibility to obtain a new physical information about hadron strong interaction from analysis of hadron-nucleus interaction features and, in particular, from investigation of secondary particle spectra behaviour.

High energy part of secondary particle spectra, e.g. hadron fragmentation region (with $x \gtrsim 0.1 \div 0.2$), is investigated at modern accelerators in more detail. The information about low energy ($x \lesssim 0.1$) hadron production off nuclei is very pure. But this region of particle momentum includes the central and nucleus fragmentation regions of rapidity spectra and is very sufficient to check the modern theoretical model calculations on hadron interaction with atomic nuclei.

From the practical point of view low energy antiproton production in high energy proton-nucleus collisions is of particular interest as a ground for antiproton source design in a scheme of $p\bar{p}$ storage rings /4/, especially, using electron cooling technique /5/.

In this paper the results of production cross section measurements of pions, protons and antiprotons at zero angle in proton-nucleus collisions at 70 GeV were presented. The cross sections were measured off Al and W targets in the following values of beam momenta 0.4,0.6,0.8 GeV/c for antiprotons, 0.4,0.6 GeV/c for protons, 0.4,0.6 and 2.0 GeV/c for positive pions and 0.4,0.6,0.8,1.07 and 2.0 GeV/c for negative pions. Pellicles of nuclear emulsion were used as a detector of the beam particles allowing to identify them by ionization measurements. Our data continue a secondary hadron spectra investigations for proton-nucleus collisions at IHEP /6/.

2. Experimental set-up and measuring procedure

The experiment was performed at high acceptance low energy single arm spectrometer at IHEP /6c,7/ (Fig. 1). The spectrometer works with the target placed in extracted from accelerator proton beam. It accepts the secondaries up to 15 mrad range of horizontal plane angle, up to 60 mrad range in vertical plane angle and has a momentum resolution equal to $\Delta p/p = \pm 1.0\%$. To prevent particles losses in the beam-line due to scattering and nuclear interaction the beam-line from target up to detector was evacuated.

In the experiment we used Al and W target of 1 cm and 0.03 cm thickness, respectively. Target thickness was choosen approximately equal to 0.1 radiation length to reduce an electron contamination in the beam. It was possible to replace the target during the exposition without switching off the magnetic elements of the spectrometer.

Proton beam profile measurements were performed by a second emission coordinate chamber (SEC) placed before the target.

We used BR-2 nuclear emulsion pellicles with a thickness of 0.5 mm as a detector of the secondary beam particles. During the exposition the pellicles were placed at the end of the beam-line, where background level was the lowest and the beam spot was smaller than the pellicle dimensions. To increase the particles track length the pellicle was placed with the angle of about 10÷15 degrees to the beam axis. The position and coordinate dimensions of the secondary beam at the pellicle were determined by proportional chamber MWPC with 2 mm anode wires spacing.

We used fast extracted proton beam in the experiment. During the exposition the proton beam intensity, namely, number of extracted proton bunches, was choosen so that a total number of secondaries crossing the pellicle didn't exceeds $2 \div 3 \cdot 10^5$. In this case it was possible to measure the grain density on the relativistic particle tracks without mixing them.

The expositions were produced at negative secondary beam momentum equal to 0.4,0.6,0.8,1.07 and 2.0 GeV/c, and at positive one equal to 0.4,0.6 and 2.0 GeV/c. To reveal a possible biases and evaluate systematics in the data we remeasured the negative particle cross sections at 0.6 GeV/c on Al and W targets. The results are statistically consistent with each other and we join the statistics at this momentum value.

3. Production cross section evaluation

The production cross section of hadron h was determined according to the formula:

$$\left.\frac{d^2\sigma_h}{dp\,d\Omega}\right|_{\theta=0^\circ} = \frac{N_h}{N_{prot} \cdot n \cdot x \cdot (dp\,d\Omega)_{eff}} \quad , \text{where}$$

N_h - number of hadron h produced in the target during the exposition, N_{prot} - number of incident protons, n - number of nuclei in cm^3 of target material, x - length of the target in cm and $(dp\,d\Omega)_{eff}$ - acceptance of the spectrometer taking into account the angular distribution of hadrons h at the target, misalignments of target and magnetic elements of the spectrometer and so on.

The determination of these quantities is described below.

3.1. Determination of hadron amounts

a) Antiprotons

To measure antiproton production cross section in this experiment the momentum values of negative secondary beam were choosen to be equal to 0.4, 0.6 and 0.8 GeV/c when the grain density on antiproton tracks approximately in 3.2 and 1.5 times exceeded the grain density a relativistic particle tracks /3/.

We scanned the every exposed pellicle by an area to find an antiproton tracks. These tracks were easy visually detected among the enormous amount of relativistic tracks crossing the

pellicle in the same direction. The every pellicle was scanned twice to find real number of antiprotons in the pellicle and a coefficient of effectiveness of individual scanning. According to these measurements the coefficiencts appear to be close to unity.

For all selected tracks we measured the grain density g^* dip angle $\alpha^{\bar{p}}$ of the track in pellicle and plane angle $\beta^{\bar{p}}$ relative to neighbouring relativistic track. The distributions of selected candidates versus g^*, angles $\alpha^{\bar{p}}$ and $\beta^{\bar{p}}$ in comparison with the distributions of relativistic particles on α^{rel} and β^{rel} are shown in Fig. 2a.

The angles α^{rel} and β^{rel} for relativistic particles characterize the angular spread of beam particles and the multiple scattering of relativistic particles in the nuclear emulsion pellicles. The arrows in Fig. 2 point out the 3 standard deviations boundaries from the means for these quantities. The standard deviation of grain density is determined by a square root of a number of grains on the tracks. The standard deviations in $\alpha^{\bar{p}}$ and $\beta^{\bar{p}}$ relative to α^{rel} and β^{rel} include the difference of multiple scattering of relativistic particles and antiprotons in the pellicle.

To check the effectiveness of g^*, $\alpha^{\bar{p}}$ and $\beta^{\bar{p}}$ selection criteria we measured the multiple scattering of the candidates relative to neighbouring relativistic particle. The obtained distribution for candidates is compared in Fig. 2b with the similar distribution for protons, obtained in measurement in the emulsion pellicle exposed in positive secondary beam of the same momentum. As it is seen from Fig. 2, the candidates N 2 and N 7 with large probability are not antiprotons. These selection criteria were used to select antiprotons in the pellicles exposed in the secondary beam of other momentum values. The selected tracks were regarded as antiprotons and were used to determine the antiproton production cross sections. The total antiproton numbers selected are listed in Table 1.

b) Pions

The pions production cross sections were measured at 0.4, 0.6,0.8, 1.07 and 2.0 GeV/c values of negative secondary beam

momentum and at 0.4, 0.6 and 2.0 GeV/c of momentum values for positive secondary beam. At these momenta the pions are relativistic with approximately minimal grain density on their tracks. Another component of the relativistic beam is muons from pion decay along the beam-line and electrons, which are the main component (~80% at 0.4 GeV/c) of the low energy "hadronic" beams.

The total numbers of relativistic particles crossed the emulsion pellicles were determined by the beam intensity profile measurements in the numerous points in the pellicle.

The total pion numbers in pellicles were obtained now by substracting the muon and electron contamination in the beam of relativistic particles. Muon component in the beam was calculated by Monte-Carlo simulation of the spectrometer by "DECAYTURTLE" computer programme. It appears to be equal to about 13% of the pions at 0.4 GeV/c and ~6% of the pions at 2.0 GeV/c.

The origin of heavy electron contamination in the low energy "hadronic", beams is neutral pions, producing gammas, which converts in e^+e pairs in the target material. To determine the electron contamination in the beam at a given momentum it is necessary to know the whole momentum spectrum of neutral pions.

We accepted the neutral pion momentum spectrum as an arithmetic mean of momentum spectrum of negative and positive pions from /6b,e/. The calculated values of $N_e/(N_e+N_\pi)$ for Al and W targets in our experiment are shown in Fig. 3. The difference in electron and pion acceptances of spectrometer due to more sharp electron angular distribution is taken into account in the calculation. The validity of the electron component calculation was performed for the emulsion pellicles exposed at 0.4 and 0.6 GeV/c secondary beams. At these values of particle momenta electrons have higher (~5÷7%) grain density on their tracks then other relativistic particles in the beam. To separate the electron tracks from others we measured the grain density on relativistic tracks in the pellicles. These measurements allowed reliably to distinguish electrons from pions and muons and to determine the electron component in the beam.

The measured grain density distributions were fitted by two gaussian peak function. The derived amplitude of the peak with the higher grain density gives the electron contamination in the relativistic beam. In Fig. 3 the comparison between calculated electron component $N_e/(N_e+N_\pi)$ and measured for positive (a) and for negative (b) secondary beam are shown. As it is seen, they are in good agreement.

The number of pions among relativistic tracks in the pellicles was derived by substraction of electrons according to calculated curves for electron contamination presented in Fig. 3. These pion numbers being corrected for pion decay along the spectrometer determine the pion production cross sections in our experiment.

However, these pion production cross sections are possibly contain a systematic error about 10%+15% due to neutral pion spectrum ambiguity.

c) Protons

The number of protons in the pellicles was determined according to beam profile histogramm for the tracks with 3 times higher grain density at 0.4 GeV/c and with 2 times higher grain density at 0.6 GeV/c relative to the minimal one.

These tracks can be easy found in the emulsion pellicle and present approximately 10% of the positive beam intensity.

3.2. The spectrometer acceptance calculation

The calculation of the spectrometer acceptance was performed by Monte-Carlo simulation of the beam channel with the help of "DECAY TURTLE" computer programme /9/. At the simulation on the proton beam profiles, measured in the experiment, misalignments of the magnetic elements and the target, and of the collimators were taken into account. The proton and antiproton angular distributions are taken flat inside the angular acceptance of the spectrometer with a good accuracy. The pion angular distribution at the target was accepted as for pp-collision analogous to work /6e/:

$$E\frac{d^3\sigma}{dp^3} \sim e^{-y^{*2}/2\sigma_\pi^2 - (m_\perp - m)/m_\pi}$$, where

$m_\perp = \sqrt{p_\perp^2 + m^2}$, m - particle mass, $p_\perp$ - transverse momentum, m_π - pion mass, y^* - particle rapidity in c.m.s. of pp-collision, σ_π^2 - pion rapidity distribution variance.

The accuracy, of the spectrometer acceptance calculations in our experiment was mainly determined by uncertainties in the target and first magnetic quads misalignment and is equal to ~10%.

3.3. Proton beam intensity measurement

The proton beam intensity N_{prot} used in the pellicle exposition was determined by measurement of proton current circulated in accelerator before the extraction of the beam. The accuracy of the proton intensity measurements was about ~ 10%. The stability of extracted proton intensity was cheked by the second-emission chamber before the target. This chamber was not separately calibrated and, therefore, the obtained in the experiment production cross sections may include a possible systematic error ~ 10% due to uncertainties of proton beam extraction coefficient.

3.4. Results

The measured production cross section of negative and positive pions, protons and antiprotons are presented in Table 2. Error bars of presented values are due to statistics, uncertainties in the spectrometer acceptance and in proton beam intensity determination. These data are possibly contain the systematic error about 20% due to factors described above.

The A-dependence of the cross sections is generally described in the form:

$$\frac{d^2\sigma}{dp\,d\Omega} \sim A^\alpha$$

The results on A-dependence measurements for pions, protons and antiprotons in this experiment are listed in Table 3. The data on production cross section ratios, namely, on proton to positive pion ratio and antiproton to negative pion ratio are shown in Table 4. The error bars of α values, determining the

A-dependence of cross sections, presented in Table 3 and particle cross section ratios, presented in Table 4, doesn't include the uncertainties in acceptance calculations, as if the exposition on Al and W targets are performed in the same conditions, and hadron cross section ratios, in addition, doesn't include the uncertainties in proton beam measurement.

4. Discussion

The data of this experiment allow to determine the pion production cross section behaviour versus lab. rapidity for central and necleus fragmentation regions in proton-nucleus collisions at 70 GeV. The rapidity spectra of positive and negative pions obtained in this experiment and from work /6e/ on Al and W targets are shown in Fig. 4. As it is seen, the yields $E\,d^3N/dp^3$ of pions increase with decreasing of pion momentum. The observed behaviour of pion rapidity spectrum produced on nucleus is to be quite natural, because every subcollision of primery proton in the nucleus and secondary hadron cascade gives a contribution in pion production to this region.

The increase of hadron yields in low rapidity region for hadron-nucleus interaction was discussed in many theoretical papers /see, for example, 1,2,3,10 and references therein/ and was established in proton-emulsion collision experiment /11/.

The conclusion about strong A-dependence of pion cross sections in low momentum region is confirmed by A-dependence measurements in this experiment. Fig. 5(a,b) showed the behaviour of power $\alpha = \ln[(E\,d^3N/dp^3)^W/(E\,d^3N/dp^3)^{Al}] / \ln(A^W/A^{Al})$ determining the A-dependence of cross sections, according to this work and work /6e/.

The A-dependence of proton and antiproton cross sections is shown in Fig. 5 (c, d). It is seen, that A-dependence of these hadrons is rather different: value of α for protons rapidly grows with proton momentum decrease to the region of proton evaporation from the nucleus, and, controversely, α value for antiprotons doesn't practically depend on momentum and equal approximately to $^2/3$, which means the yield equality in proton collisions with heavy and light nucleus.

The dependence of $R = (\bar{p}/\pi^-)^W / (\bar{p}/\pi^-)^{Al}$ from this work and work /6e/, as a function of particle momentum, is shown in Fig. 6. As it is seen, the antiproton to pion ratio $(\bar{p}/\pi^-)$ practically is independent of atomic weight of nucleus in this momentum region. Similar results on this ratio were obtained in the work /12/, investigated proton-nucleus collisions at 10 GeV. The authors interpretate their results as an evidence for weak antiproton absorption inside the nucleus.

The momentum dependence of p/π^+ and $\bar{p}/\pi^-$ -ratios are presented in Fig. 7. The proton to positive pion ratio (p/π^+) increases with decreasing of particle momentum and strongly depends on atomic weight of the nucleus. The antiproton to negative pion ratio $(\bar{p}/\pi^-)$ decreases in the same way as antiproton yield with particle momentum decreasing.

In conclusion authors express their gratitude to S.S.Gerstein, I.I.Gurevich, A.N.Skrinsky and V.A.Jarba for attention and support of this work, and to O.V.Zhirov for numerous useful discussions.

References

1. Yu.P.Nikitin et al., Uspekhi Fiz. Nauk, 121 (1973), 3.
2. N.N.Nikolaev, Uspekhi Fiz. Nauk, 134 (1981), 3.
3. Yu.M.Shabelski, Particles and Nucleus, 12 (1981), 5.
4. T.A.Vsevolozhskaja et al., preprint INP 80-182, Novosibirsk, 1980, Proc. of the USSR Meeting on Accelerators, Dubna, 1981.
5. G.I.Budker, A.N.Skrinsky, Uspekhi Fiz. Nauk, 124(1974), 4. A.N.Skrinsky, V.V.Parkhomchuk, Particles and Nucleus, 12 (1981), 4.
6. a) F.Binon et al., Phys. Lett., 30B (1969), 506.
   b) N.I.Bozhko et al., preprint IHEP 79-78, Serpukhov, 1979.
   c) L.M.Barkov et al., preprint IHEP 79-92, Serpukhov, 1979.
   d) V.V.Abramov et al., preprint IHEP 79-131, Serpukhov, 1979.
   e) L.M.Barkov et al., preprint IHEP 81-107, Serpukhov, 1981.
7. V.I.Kotov et al., Proc. of the USSR meeting on accelerators, Dubna, 1981.
8. V.V.Ogurtzov, thesis, Moscow, 1971.
9. K.L.Brown et al., preprint CERN 74-2, 1974.
10. L.Ber ..chi, Proc. 6-th Intern. Conf. on High Energy Physic and Nucl. Structure, Santa Fe, 211, 1975. W Buzsa, ibid, p. 238.
11. S.A.Azimov et al., Phys. Lett., 73B (1978), 500.
12. A.O.Vaisenberg et al., Pisma v ZhETF, 29 (1979), 719.

Figure captions

Fig. 1. a) The spectrometer arrangement: $Q_{1\div4}$ - magnetic quads, $M_{1\div2}$ - magnets, IC - collimator, defining the momentum resolution of the spectrometer, T - target, SEC - secondary emission chamber, BR-2 - nuclear emulsion pellicle, MWPC - proportional chamber.

b) Beam envelope in the spectrometer.

Fig. 2. a) The candidates distributions on grain density g^* (in units of relativistic track grain density), on dip angle $\alpha^{\bar{P}}$ and on plane angle $\beta^{\bar{P}}$ in comparison with α^{rel} and β^{rel} for relativistic tracks.

c) Multiple scattering measurements on candidates and proton-tracks. $\sqrt{\langle \mathfrak{D}^2 \rangle}$ - track square displacement (microns).

Fig. 3. a) Positron component $N_{e^+}/(N_{e^+} + N_{\pi^+})$ in positive secondary beam calculated for Al and W targets of our experiment in comparison with obtained in grain density measurements on relativistic tracks.

b) The electron component in the negative particle beam.

Fig. 4. The invariant multiplicity dependence on rapidity for positive (a) and negative (b) pions.

Fig. 5. The power α of A-dependence versus particle momentum derived by cross section ratios on W and Al targets for positive (a) and negative (b) pions, for protons (c) and antiprotons (d).

Fig. 6. The A-dependence of antiproton to negative pion ratio versus particle momentum.

Fig. 7. The ratios of protons and positive pions (a) and antiprotons and negative pions (b) versus particle momentum.

Table 1. The antiproton numbers detected in this experiment.

Target \ P(GeV/c)	0.4	0.6	0.8
W	0	15	-
Al	2	11	20

Table 2. The hadron production cross sections.

a) Negative particles

P (GeV/c)	Target	$\frac{d^2\sigma}{dp\,d\Omega}\Big\|_{\theta=0^\circ}$ (barn/GeV/c·sr·nucleus) pions	antiprotons
0.4	W	3.58 ± 0.57	$\leq 3.6 \cdot 10^{-5}$
	Al	$(6.44 \pm 1.09) \cdot 10^{-1}$	$(1.9 \pm 1.3) \cdot 10^{-5}$
0.6	W	(4.39 ± 0.96)	$(2.04 \pm 0.70) \cdot 10^{-4}$
	Al	$(8.44 \pm 1.85) \cdot 10^{-1}$	$(3.50 \pm 1.33) \cdot 10^{-5}$
0.8	Al	$(8.18 \pm 1.48) \cdot 10^{-1}$	$(7.36 \pm 1.99) \cdot 10^{-5}$
1.07	W	(4.37 ± 1.09)	-
2.0	W	(6.01 ± 1.00)	-
	Al	(1.39 ± 0.22)	-

b) Positive particles

	Target	$\frac{d^2\sigma}{dp\,d\Omega}\Big\|_{\theta=0^\circ}$ (barn/GeV/c·sr·nucleus) pions	protons
0.4	W	2.87 ± 0.43	1.41 ± 0.23
	Al	$(5.35 \pm 0.96) \cdot 10^{-1}$	$(1.93 \pm 0.37) \cdot 10^{-1}$
0.6	W	3.24 ± 0.88	1.35 ± 0.27
	Al	$(6.58 \pm 1.32) \cdot 10^{-1}$	$(1.14 \pm 0.19) \cdot 10^{-1}$
2.0	W	7.66 ± 1.07	-
	Al	1.60 ± 0.24	-

Table 3. The power α of A-dependence of π , p and $\bar{p}$ cross sections

	Positive particles			Negative particles		
P(GeV/c)	0.4	0.6	2.0	0.4	0.6	2.0
$\alpha_{\pi^\pm}$	0.88 ± 0.11	0.83 ± 0.18	0.81 ± 0.12	0.87 ± 0.12	$0.84^{+0.14}_{-0.20}$	0.74 ± 0.12
$\alpha_{p,\bar{p}}$	1.01 ± 14	1.21 ± 0.14	-	-	$0.89^{+0.18}_{-0.27}$	-

Table 4. Hadron yield ratios

	p/π^+		$\bar{p}/\pi^-$		
P(GeV/c) / Target	0.4	0.6	0.4	0.6	0.8
W	0.49 ± 0.04	0.42 ± 0.04	$\leq 1.0 \cdot 10^{-5}$	$(4.64 \pm 1.29) \cdot 10^{-5}$	-
Al	0.36 ± 0.05	0.17 ± 0.02	$(2.95 \pm 2.10) \cdot 10^{-5}$	$(4.17 \pm 1.49) \cdot 10^{-5}$	$(9.02 \pm 2.17) \cdot 10^{-5}$

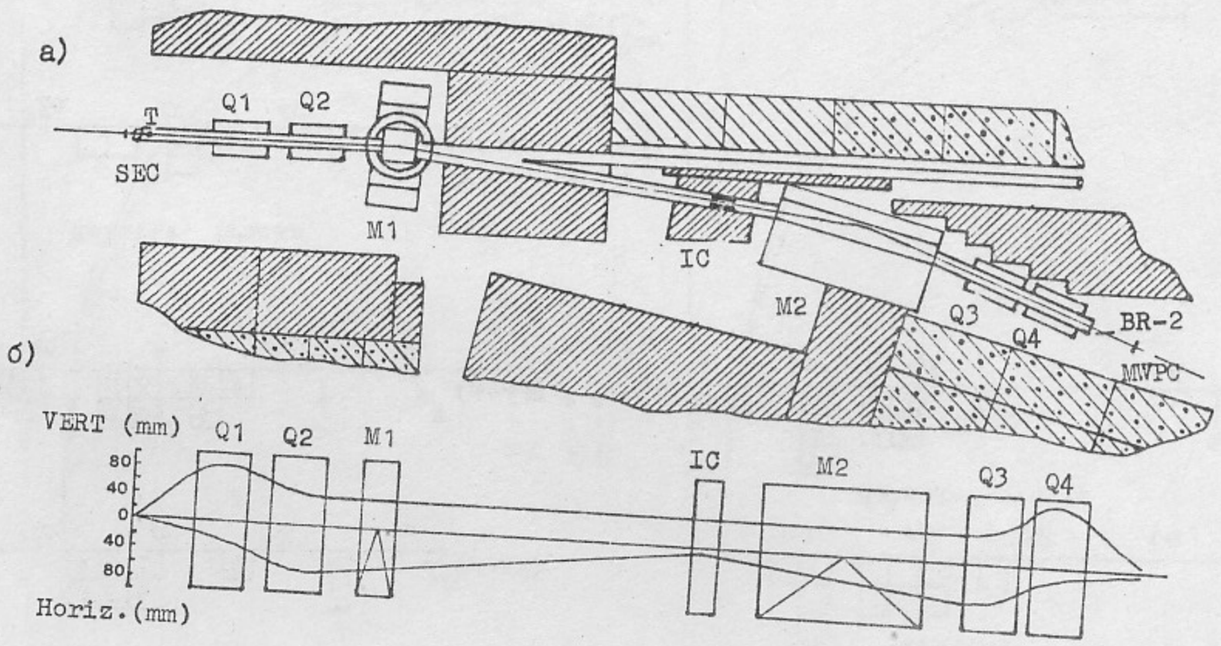

Fig. 1

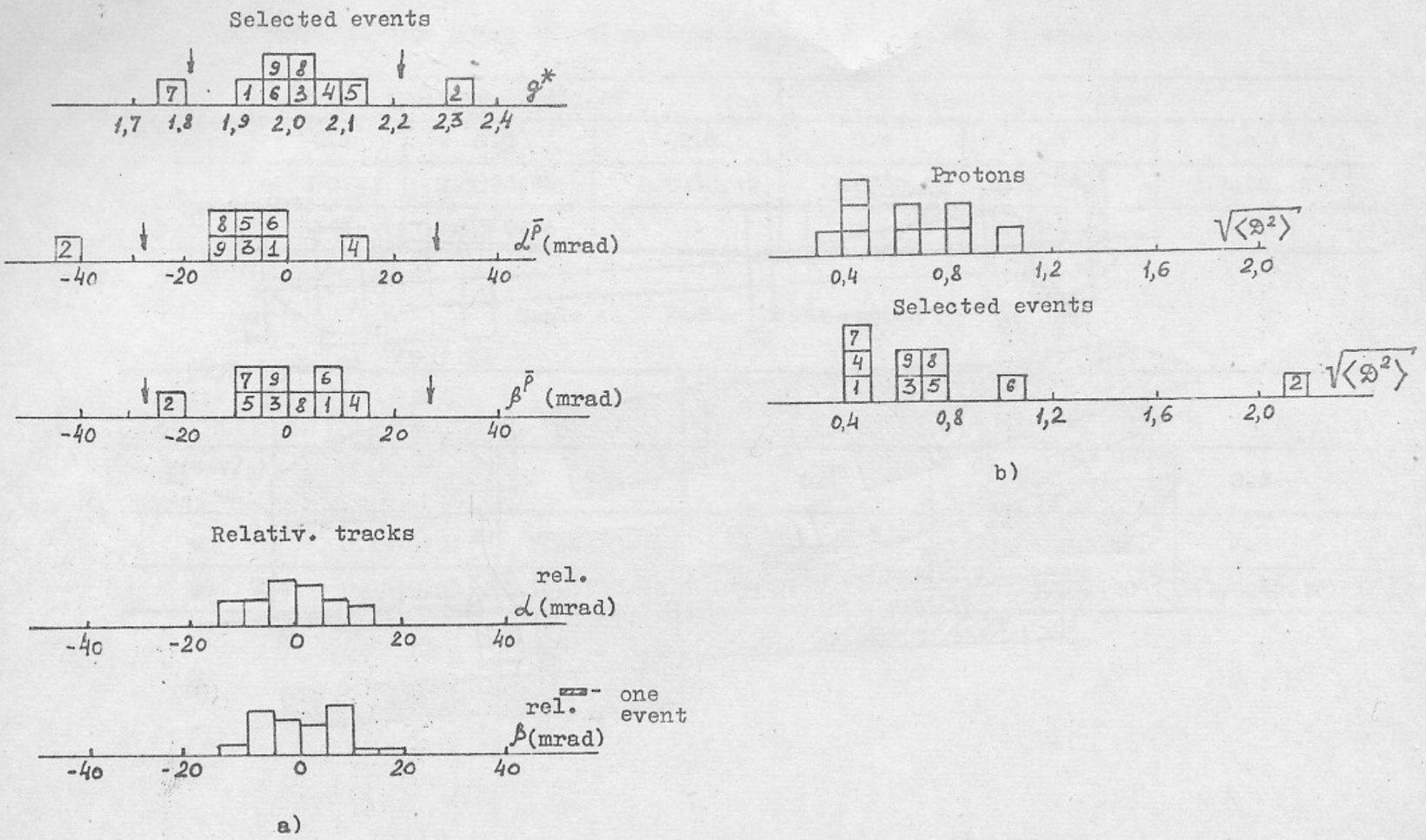
Selected events
g*
1,7 1,8 1,9 2,0 2,1 2,2 2,3 2,4
(mrad)
-40 -20 0 20 40
(mrad)
-40 -20 0 20 40
Relativ. tracks
rel.
(mrad)
-40 -20 0 20 40
rel.
one event
(mrad)
-40 -20 0 20 40
a)
Protons
0,4 0,8 1,2 1,6 2,0
Selected events
0,4 0,8 1,2 1,6 2,0
b)

Fig. 2

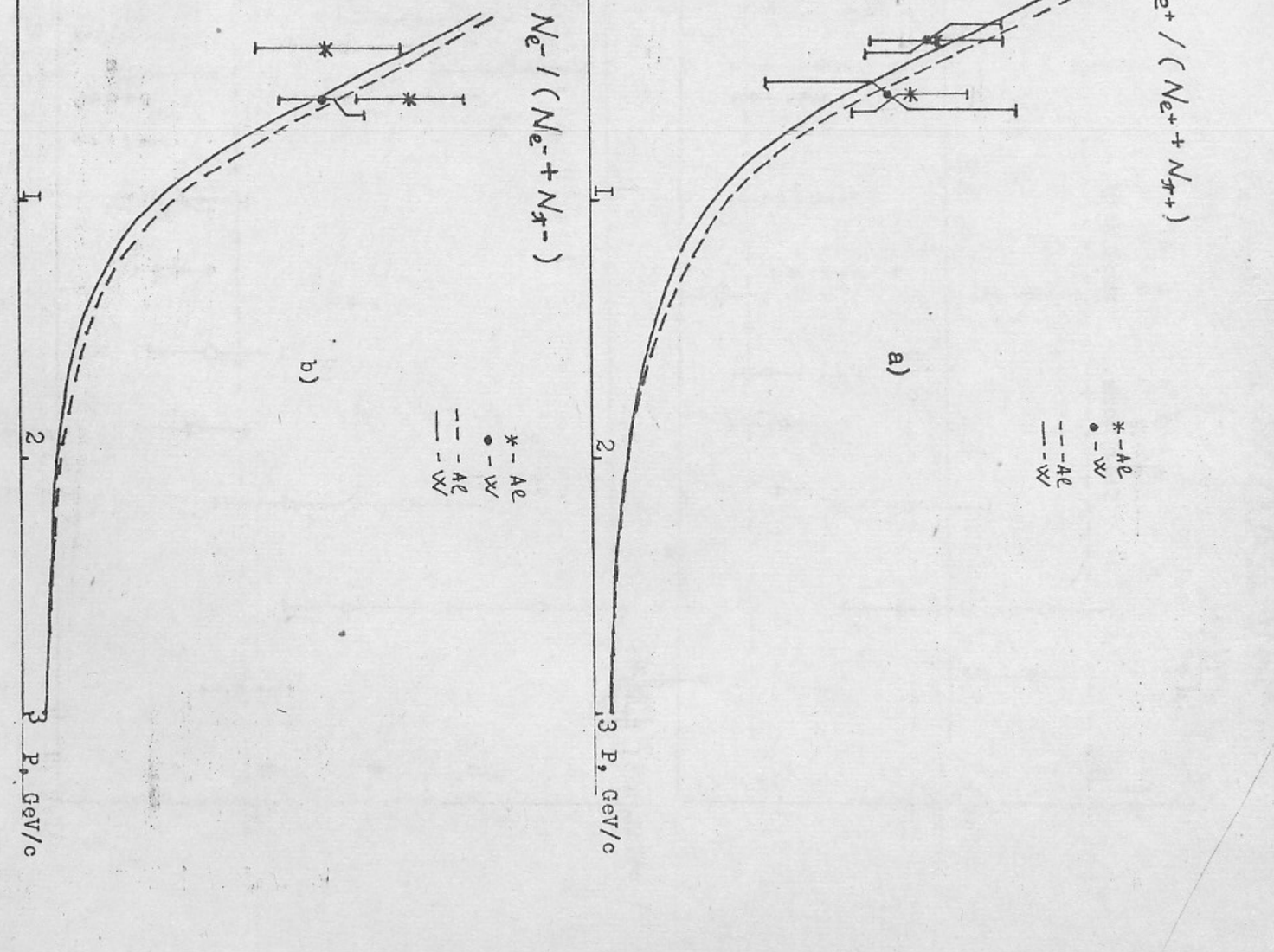
I,0
0,5
a)
I,0
0,5
b)
*-Ae
•-W
---Ae
——W
I, 2, 3 P, GeV/c

Fig. 3

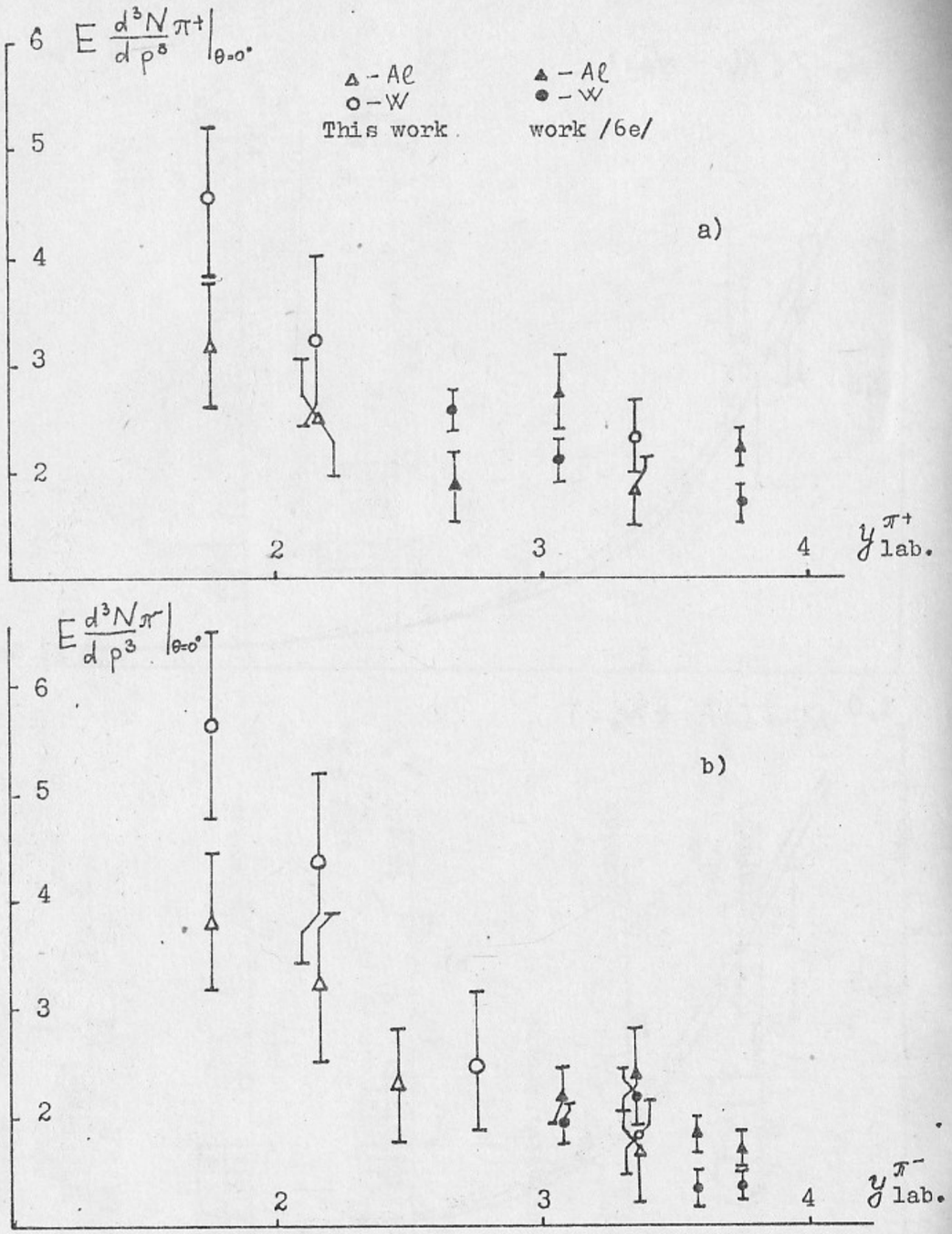
$E\frac{d^3N\pi^+}{dp^3}\Big|_{\theta=0^\circ}$
△ - Al
○ - W
This work
▲ - Al
● - W
work /6e/
a)
$y^{\pi^+}_{lab.}$
$E\frac{d^3N\pi^-}{dp^3}\Big|_{\theta=0^\circ}$
b)
$y^{\pi^-}_{lab.}$

Fig. 4

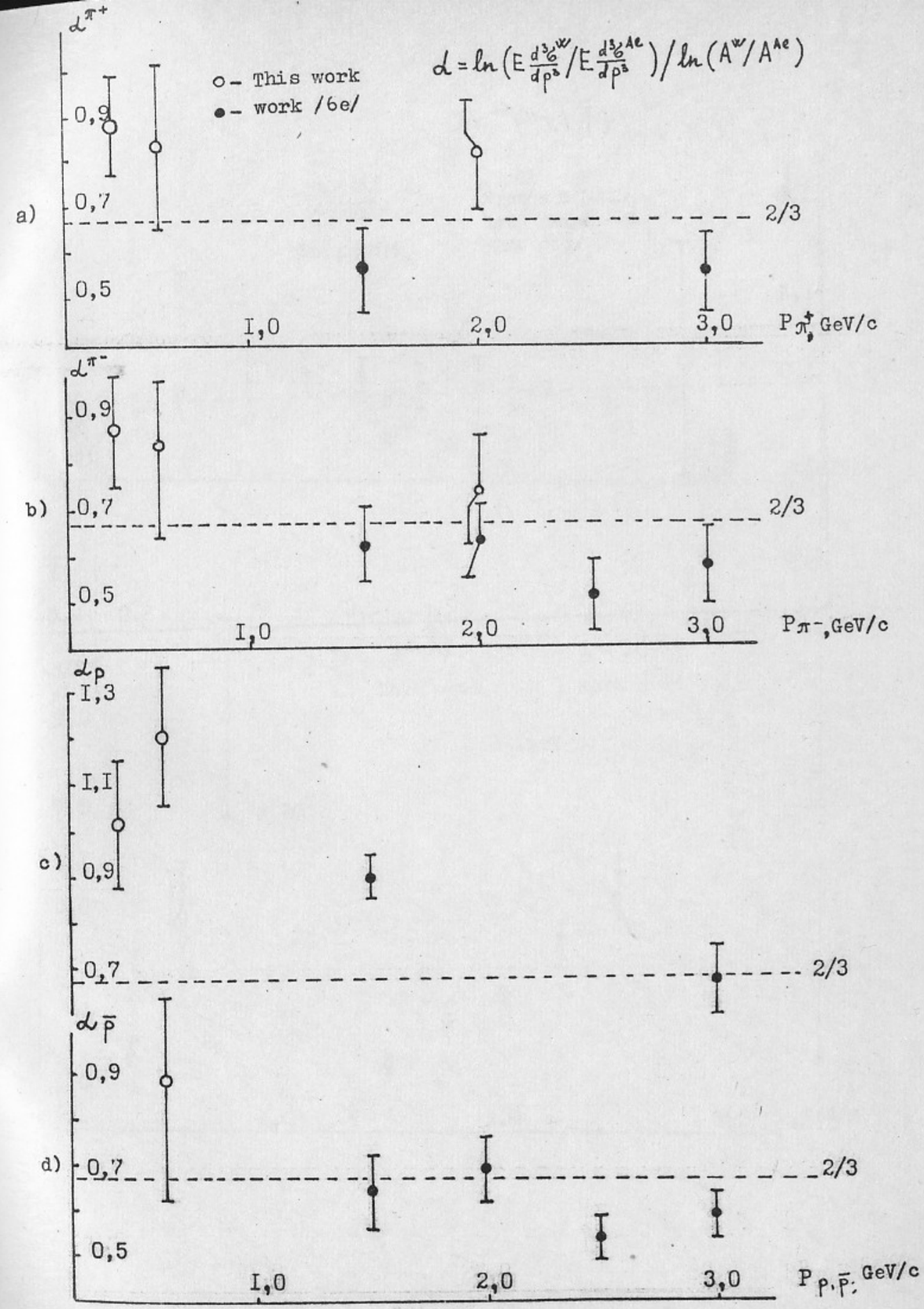
α^{π^+}
○ - This work
● - work /6e/
$\alpha = \ln\left(E\frac{d^3\sigma^W}{dp^3}/E\frac{d^3\sigma^{Al}}{dp^3}\right)/\ln(A^W/A^{Al})$
a)
2/3
P_{π^+}, GeV/c
α^{π^-}
b)
P_{π^-}, GeV/c
α_p
c)
$\alpha_{\bar{p}}$
d)
$P_{p,\bar{p}}$, GeV/c

Fig. 5

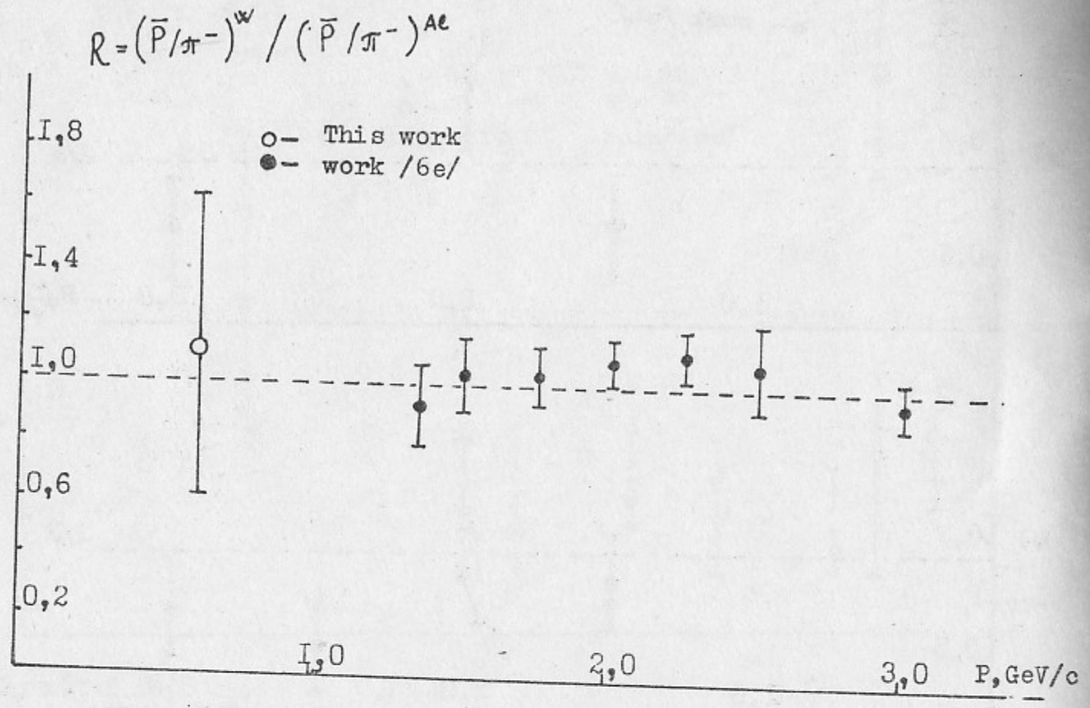
R = (P̄/π⁻)^W / (P̄/π⁻)^Al
I,8
I,4
I,0
0,6
0,2
This work
work /6e/
I,0
2,0
3,0
P,GeV/c

Fig. 6

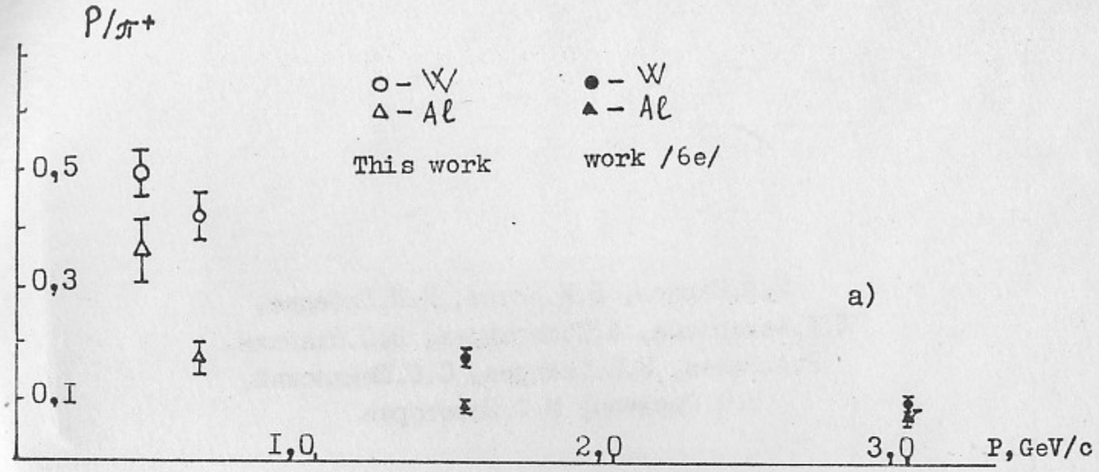
P/π+
○ - W
△ - Al
● - W
▲ - Al
This work
work /6e/
0,5
0,3
0,I
a)
I,0
2,0
3,0
P,GeV/c

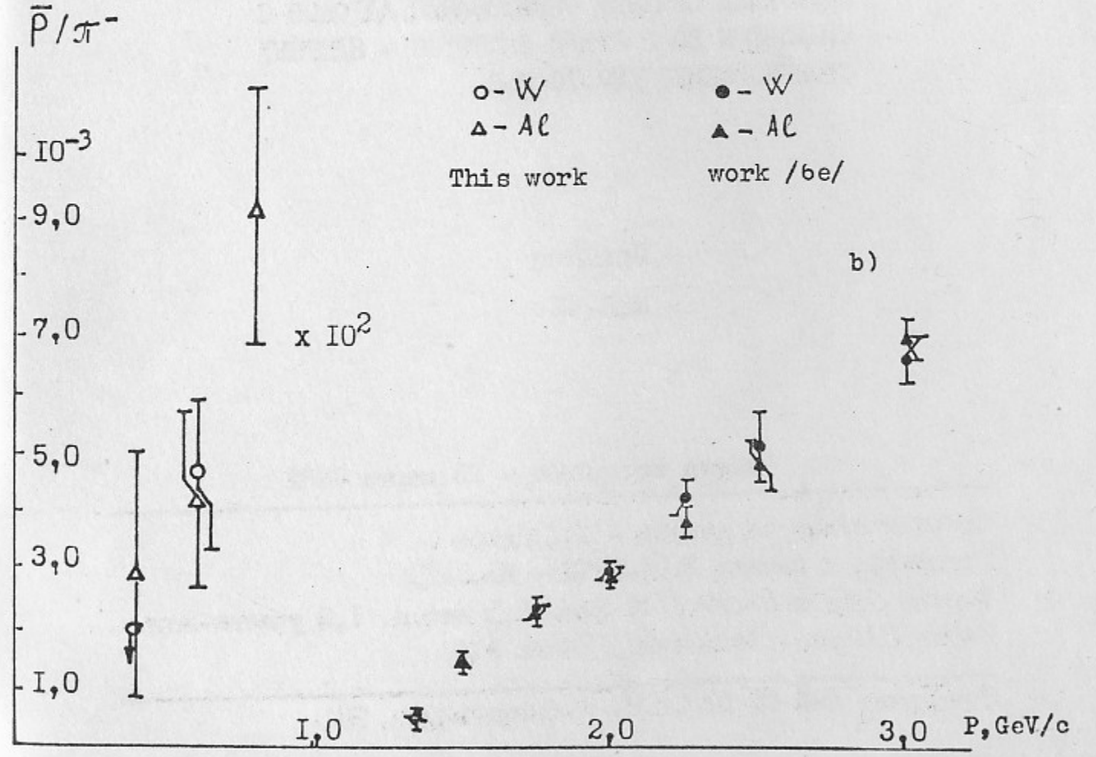
P̄/π⁻
○ - W
△ - Al
● - W
▲ - Al
This work
work /6e/
IO⁻³
9,0
7,0
x IO²
5,0
3,0
I,0
b)
I,0
2,0
3,0
P,GeV/c

Fig. 7

Л.М.Барков, В.И.Котов, П.К.Лебедев,
Л.А.Макарьина, А.П.Мишакова, В.С.Охапкин,
Р.А.Рзаев, В.П.Сахаров, С.С.Шиманский,
В.П.Смахтин, М.С.Золоторев

ИЗМЕРЕНИЕ СЕЧЕНИЙ ОБРАЗОВАНИЯ АДРОНОВ С ИМПУЛЬСОМ ДО 2 ГэВ/с В ПРОТОН - ЯДЕРНЫХ СТОЛКНОВЕНИЯХ ПРИ 70 ГэВ

Препринт
№82-42

Работа поступила - 25 марта 1982

Ответственный за выпуск - С.Г.Попов
Подписано к печати 2.04-1982г. МН 03196
Формат бумаги 60x90 1/16 Усл. 1,5 печ.л. 1,2 учетно-изд.л.
Тираж 290 экз. Бесплатно, Заказ № 42.

Ротапринт ИЯФ СО АН СССР, г.Новосибирск, 90